Ligand-Linked Structural Transitions in Crystals of a Cooperative Dimeric Hemoglobin†

James E. Knapp and William E. Royer, Jr.*

Department of Biochemistry and Molecular Pharmacology, University of Massachusetts Medical School, Worcester, Massachusetts 01605

Received November 7, 2002; Revised Manuscript Received February 13, 2003

ABSTRACT: Cooperative ligand binding in the dimeric hemoglobin (HbI) from the blood clam *Scapharca inaequivalvis* is mediated primarily by tertiary structural changes, but with a small quaternary rearrangement (∼3°), based on analysis of distinct crystal forms for ligated and unligated molecules. We report here ligand transition structures in both crystal forms. Binding CO to unligated HbI crystals results in a structure that approaches, but does not attain, the full allosteric transition. In contrast, removing CO from the HbI−CO crystals results in a structure that possesses all the key low affinity attributes previously identified from analysis of HbI crystals grown in the unligated state. Subsequent binding of CO shows the reversibility of this process. The observed structural changes include the quaternary rearrangement even under the constraints of lattice interactions, demonstrating that subunit rotation is an integral component of the ligand-linked structural transition in HbI. Analysis of both crystal forms, along with data from HbI mutants, suggests that the quaternary structural change is linked to the movement of the heme group, supporting a hypothesis that the heme movement is the central event that triggers cooperative ligand binding in this hemoglobin dimer. These results show both the effects of a crystal lattice in limiting quaternary structural transitions and provide the first example of complete allosteric transitions within another crystal lattice.

Allosteric regulation depends on ligand-linked structural transitions that serve to alter the functional properties of the protein. For alternate allosteric conformations to be accessible under physiological conditions, they must be separated by relatively small energetic differences. For instance, the difference in quaternary stability between the oxygenated and deoxygenated forms of human hemoglobin is about 6 kcal/mol, equivalent to only a couple of hydrogen bonds (*1*). Given such small differences, a plausible concern in the crystallographic analysis of allosteric proteins is that crystal lattice interactions or solvent conditions could significantly perturb the observed structures. Evidence of such effects is found in the structure of ligated human hemoglobin, for which quite different quaternary forms are observed in crystals grown under distinct conditions (*2*−*4*). Consequently, the structural basis for allosteric regulation would ideally be investigated under conditions without the complication of different crystal lattices or solvent conditions, such as following structural transitions within a single-crystal lattice. However, following structural changes for a protein that undergoes large quaternary changes will often be incompatible with the crystal lattice, as experiments on human hemoglobin have indicated (*5*, *6*).

The dimeric hemoglobin (HbI)[1] from the blood clam *Scapharca inaequivalvis* is an exceptional model system in which to study protein allostery. Allostery is present in HbI as cooperative ligand binding as identified by both equilibrium and kinetic experiments (*7*, *8*). Although the two identical subunits of HbI are folded similarly to subunits in mammalian hemoglobins, their assembly into a cooperative complex is quite different. The HbI assemblage brings the heme groups close together, permitting cooperativity to be mediated primarily by tertiary changes, rather than large quaternary rearrangements as in vertebrate hemoglobin and other allosteric proteins. Despite rather localized ligand-linked structural changes, there is strong modulation of the ligand affinity; the oxygen affinity of the R-state is estimated to be ∼300 times higher than that of the T-state molecule, based on analysis of the kinetic ligand binding parameters in the context of the concerted MWC model (*9*, *10*). The limited subunit rotations (∼3°) observed from comparison of structures for ligated and unligated HbI in distinct crystal lattices (Figure 1) suggest that structural transitions underlying allostery might be followed in the crystalline lattice. Such a possibility was raised by the report of full cooperativity in oxygen equilibrium experiments with crystals grown from unligated HbI (*11*).

We present here transition structures obtained by altering the state of ligation in crystals of HbI grown both under unligated and CO-ligated conditions. Binding of CO to previously unligated HbI crystals resulted in a structure that approaches, but does not attain, the structure observed in crystals grown in the ligated state. In contrast, structures obtained by removal, and also by subsequent rebinding, of CO to crystals of HbI grown in the CO-ligated state show that full and reversible allosteric transitions are compatible with this lattice. These transitions include both tertiary and quaternary structural changes, demonstrating that the small

† This work is supported by NIH Grant DK43323 to WER, and by a postdoctoral fellowship from the New England Affiliate of the American Heart Association to JEK.

* To whom correspondence should be addressed. Telephone: (508) 856-6912. Fax: (508) 856-6464. E-mail: william.royer@umassmed.edu.

[1] Abbreviations: Hb, hemoglobin; HbI, hemoglobin I; CO, carbon monoxide; rms, root-mean-square.

10.1021/bi027136p CCC: $25.00
Published on Web 04/01/2003

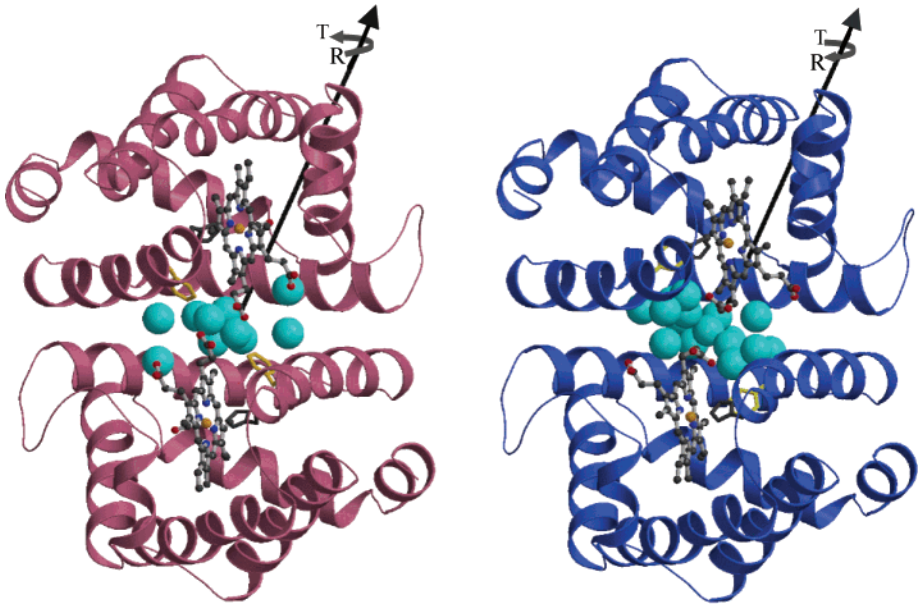

FIGURE 1: Schematic diagram showing the changes of HbI as it goes from a ligated R-state (left, PDB code 3SDH) to an unligated T-state (right, PDB code 4SDH). The A (lower) subunit from the R-state has been superimposed upon the A subunit of the T-state, and the axis defining the pivot point around which the B-subunit reorientates by 3.3° is defined by the black arrow. This figure also shows the major tertiary changes that are linked to ligand binding, including the movement of the heme group, that of Phe 97 (shown in yellow), and the rearrangement of the water molecules at the interface. (Figure produced with MOLSCRIPT (*35*) and RASTER3D (*38*).)

Table 1: Crystallographic Data on HbI Transition Crystals

	T to CO transition	R-deligation transition crystals	double transition (CO to deoxy to CO)
space group	$C222_1$	$P2_1$(alternate cell)	$C2$
a (Å)	92.0	83.8 (91.4)	92.6
b (Å)	44.3	44.2 (44.2)	43.5
c (Å)	144.0	87.1 (83.8)	83.1
β (°)	90	115.5 (120.6)	121.9
mosaicity (°)	0.63	1.6	2.2
resolution (overall)	40.0−1.85 Å	40.0−2.5 Å	40.0−2.8 Å
high-resolution shell	1.92−1.85 Å	2.59−2.50 Å	2.90−2.80 Å
reflections	24623	19646	6301
observations	82801	75147	15137
completeness[a]	95.2 (87.8)	95.3 (85.5)	85.6 (74.1)
Rsym[a]	8.4 (32.1)	7.7 (23.9)	9.6 (26.1)
I/σ (I)	12.0	11.5	9.1
R-factor[a]	0.189 (0.303)	0.194 (0.235)	0.221 (0.320)
R-free[a]	0.210 (0.290)	0.218 (0.241)	0.249 (0.398)
RMS deviation from ideal values			
bonds lengths	0.006 Å	0.005	0.011
bond angles	1.00°	1.15	1.31
Ramachandran plot %			
most favored regions	94.7	94.3	95.0
allowed regions	5.3	5.7	5.0

[a] Values in parentheses refer to the high resolution shell.

reorientation of the two subunits is integral to the cooperative transition of HbI. To our knowledge, this is the first demonstration of a cooperative protein that can undergo complete allosteric transitions within a crystalline lattice.

MATERIALS AND METHODS

Materials. Potassium ferricyanide and potasium cyanide were obtained from Sigma Aldrich. Sodium hypodisulfite (sodium dithionite) was obtained from Hoechst-Celanese. *Scapharca inaequivalvis* dimeric HbI was expressed, purified, and crystallized in the CO-ligated and unligated states as described previously (*12*, *13*).

Unligated to CO Transition. Unligated HbI crystals were mounted in capillary tubes in a Bactron II anerobic chamber (Anaerobe Systems, Morgan Hill, CA). A single diffraction image was recorded with a R-axis IV detector system (Molecular Structure Corp., The Woodlands, TX) equipped with a Rigaku RU300 rotating anode X-ray source and osmic mirrors. This image demonstrated the quality of the crystal and the $C222_1$ space group symmetry. The capillary tube was cut open, and the crystal was exposed to a CO stream for 30 s. The capillary tube was resealed, and the crystal was allowed to equilibrate with the CO for 12 days. The bright red color of the crystal indicated successful CO binding before X-ray diffraction data were collected. A total of 90 images were collected and then processed and merged in the HKL package (*14*) (Table 1). This data set still exhibited $C222_1$ symmetry, with cell constants that are similar to unligated HbI.

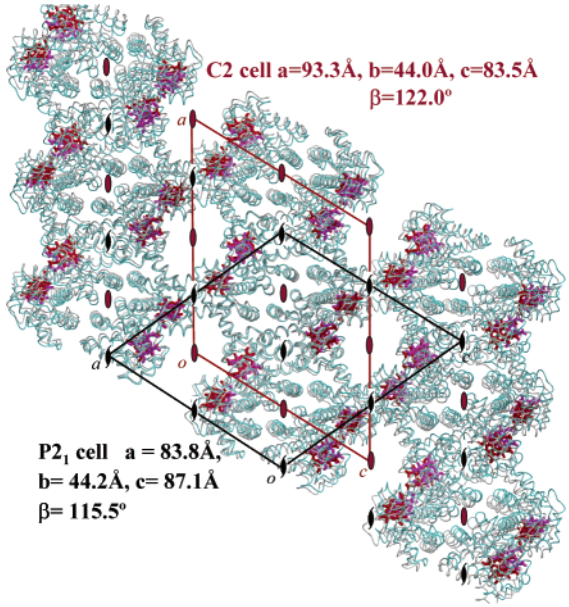

FIGURE 2: Packing diagram of the monoclinic HbI−CO crystal form viewed along the *b* axis. Eighteen HbI−CO dimers are depicted as gray α-carbon traces with red hemes, while the structure of 18 dimers following removal of CO are shown in cyan. Approximate positions of crystallographic 2-fold axes along *b* are shown as red ovals and the 2-fold screw axes in black. Removal of CO results in the loss of the crystallographic 2-fold operators, but retention of the 2-fold screw operators, such that the cell now has $P2_1$ symmetry. Outline of the C2 cell is shown in red, and that of the conventional $P2_1$ cell is shown in black. (An alternate $P2_1$ cell can be defined that is similar to the C2 cell but has its origin shifted by 1/4 of a unit cell edge along a.) Note that the quaternary structural differences between the two states of HbI do not greatly alter the packing of the molecules within the crystal lattice. (Figures 2, 4, and 5 were prepared with MIDAS (*36*).)

CO Deligation Transition. CO ligands were initially displaced by soaking crystals in a solution containing 150 mM potassium ferricyanide, 300 mM potassium cyanide, 2.2 M phosphate at pH 7.5 for 2 h under a light source. This solution oxidized the heme group within HbI crystals to the cyanomet derivative. The oxidized HbI crystals were then rinsed in a stabilizing solution of 2.2 M phosphate at pH 7.5 and transferred into our anaerobic chamber. Crystals were reduced in this chamber by soaking them in a solution of 150 mM sodium dithionite and 2.2 M phosphate (pH 7.5) for between 2 and 6 h. Crystals were then mounted in capillary tubes and sealed with epoxy. X-ray diffraction data were collected on a Raxis IIc image plate system equipped with a Rigaku RU200 generator and Yale mirrors (Molecular Structure Corp., The Woodlands, TX). Data collected from crystals that were deligated in this manner revealed a transformation from the *C*2 cell of the CO-ligated crystals to the closely related primitive monoclinic $P2_1$ cell (Figure 2). The diffraction images were processed and merged as described above (Table 1).

Attempts were also made to photolytically remove the CO ligand from HbI−CO crystals. In these experiments, crystals were exposed to air under a bright light source for 4 h then transferred into the anaerobic chamber where they were soaked in a solution of 100 mM dithionite in 2.2 M phosphate buffer pH 7.5. Diffraction data from these crystals were measured with the Raxis IIc system and found to be isomorphous to crystals of HbI−CO. The $2F_o - F_c$, σ^A weighted electron density maps shows clear density for a diatomic ligand bound to the heme iron. However, $F_{o\ (native)} - F_{o(light/reduction)}$ difference maps indicate that a small fraction of CO ligand is no longer bound to the heme, suggesting partial success with this alternative procedure.

CO Double Transition. Two crystals that underwent the above oxidation−reduction protocol were mounted in capillary tubes under anaerobic conditions. For each crystal, a single frame was collected, which indexed in HKL (*14*) as the $P2_1$ lattice of the unligated transition crystals. The capillaries were then cut, the crystal was exposed to carbon monoxide for 20 s, and the capillary tube resealed. Observation of the crystals under a microscope verified that they had turned from dark purple to bright red indicative of the CO ligation state. After a 30 min incubation time, a total of 100 frames were collected from the first crystal. The second crystal was equilibrated with CO for 24 h in a sealed capillary tube before data collection. The first 19 frames as well as frames 23 and 26 from the first crystal indexed in the $P2_1$ lattice of the deoxy transition crystals whereas all other frames from the first crystal and all frames from the second crystal indexed in the C2 lattice of the HbI−CO crystals. The merged data set includes frames 41−69 from the first crystal and frames 1−61 from the second crystal. It should be noted that each transition decreases the effective resolution of the diffraction and sequentially increased crystal mosaicity (Table 1).

Analysis of the Crystal Structures. Before refinement, 5% of the data were set aside to calculate a free R-factor. Molecular replacement phases for the unligated to CO transition were calculated from the unligated HbI structure (PDB code 4SDH) with the side chains of Lys 96, Phe 97, and Asn 100 truncated to alanine. The HbI−CO structure (PDB code 3SDH), also omitting the side chains of Lys 96, Phe 97, and Asn 100 and the CO ligand, was used to phase both the single and double transition data sets. The initial model was placed into the single transition ($P2_1$) cell using the molecular replacement routine of EPMR (*15*).

All three models were optimized with multiple rounds of CNS refinement (*16*) followed by manual adjustments with O (*17*). The unligated to CO transition included individual B-factor refinement and alternate conformations. The other two transition structures included the optimization of group main chain and side chain B-factors for each residue and the averaging of B-factors between equivalent residues of the two subunits. This latter step was done with MOLEMAN (*18*). Water molecules were added to peaks in a $F_o - F_c$ difference map and were retained if they had good stereochemistry and reasonable density in a $2F_o - F_c$, σ^A weighted omit map. The model of the deligated CO−HbI crystals has an average coordinate error of between 0.29 and 0.31 Å as calculated by cross-validated σ^A and Luzati plots. The same treatment for the double transition data gives estimated errors between 0.40 and 0.51 Å. The structure of the unligated to CO form has an estimated coordinate error between 0.21 and 0.23 Å.

Least squares superposition calculations were made with LSQMAN (*19*) using the Cα atoms between residues 10 and 146 because the first nine residues are flexible. Subunit rotations between ligated and unligated state were defined by first superimposing the A subunits of the two states, followed by calculation of the rotation necessary to super-

Table 2: Structural Parameters of HbI in Its Various States

	R-state	T-state	T-state to CO	R-state to deoxyAB	R-state to deoxyCD	double transition
RMS subunit superposition to the R-state (Å)[a]	0.22	0.38	0.28	0.36	0.37	0.18
RMS subunit superposition to the T-state (Å)[a]	0.38	0.18	0.21	0.24	0.19	0.40
subunit rotation to the R-state (°)	0.0	3.3	2.9	2.2	4.1	1.0
subunit rotation to the T-state (°)	3.3	0.0	0.6	1.3	0.8	4.1
Fe to heme plane distance (Å)	0.039	0.52	0.10	0.50	0.55	0.028
rms heme plane (Å)	0.098	0.15	0.091	0.14	0.14	0.093
Fe_A-Fe_B distance (Å)	18.4	16.6	18.0	16.7	16.7	18.4
Phe 97 O−Nδ1 His 101 (Å)	2.8	3.1	3.2	3.2	3.2	2.9

[a] These values represent the average root-mean-square (rms) difference calculated from the superposition of 137 Cα atoms (residues 10−146) from each subunit of one model onto each subunit of either the T-state (unligated) and R-state (CO-ligated) forms of HbI. In the case of the R-state superimposed upon the R-state and the T-state on the T-state, these calculations represent the differences between the two subunits of a dimer.

impose the B subunits. The calculation of planes was made with Geomcalc of the CCP4 package (*20*), and included the atoms of the four pyrrole rings and the four bridging methylene carbons. The unligated to CO transition coordinates have been deposited in the Protein Data Bank (*21*) under the accession code 1NXF. The coordinates of the HbI−CO single (1NWI) and double transition (1NWN) structures are also available at the Protein Data Bank (*21*).

RESULTS AND DISCUSSION

Previous analyses of the cooperative ligand-linked structural transitions for *Scapharca* HbI were based on comparisons between distinct crystal lattices grown in ligated and unligated states. Crystals of HbI ligated with either CO or O_2 show the symmetry of the C-centered monoclinic space group *C*2 with one dimer per asymmetric unit, whereas those of unligated HbI show the symmetry of the orthorhombic space group $C222_1$ also with one dimer per asymmetric unit (*13*, *22*). In the descriptions to follow, the conformations observed from these earlier structural determinations will be referred to as R-state (CO or O_2 ligated) or T-state (unligated).

T-State to CO Transition. An unligated HbI crystal exposed to CO while mounted in a thin-walled glass capillary maintained sufficient internal order to allow collection of a diffraction data set to 1.85 Å resolution (Table 1). Confirmation that CO has successfully bound at the heme sites is shown in Figure 3D. The refined model for this transition structure shows that the heme group attains the geometry expected for ligation, with the iron in the heme plane and the heme much more planar than in the deoxy structure (Table 2).

Carbon monoxide binding induces a number of tertiary changes that give rise to a ligated structure, but for which the full allosteric transitions are attenuated. Ligation in the crystal lattice results in a 0.6° rotation of subunits, significantly less than the 3.3° observed from a comparison of the two lattices (Figure 4). The heme groups move toward their R-state position (Table 1), but the A propionate side groups from both hemes remain folded back in a T-state conformation (Figure 5a). Amino acid side chains involved in key contacts at the heme or dimer interface show aspects of both R- and T-state conformations. Arg 53 adopts a position that is between its counterparts in the R- and T-states, Asn 100 and Arg 104 move near to their respective R-state conformation while Phe 97 and Lys 96 show alternate conformations that correspond to both the R- and T-states (Figure 5a). The core water structure at the subunit interface is R-like with

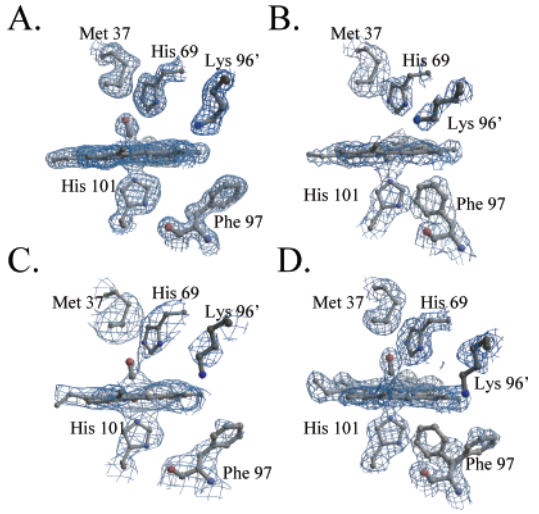

FIGURE 3: Electron density maps of HbI−CO and transition structures. HbI−CO exhibits an R-state structure (A) but converts to a T-state structure when ligands are lost (B), and back to the R-state when CO is added back (C). Addition of CO to unligated HbI results in a partial transition to the R-state with Phe 97 and Lys 96 occupying both R- and T-state positions (D). Each model is superimposed upon a $2F_o - F_c$, simulated annealing omit map contoured at either 0.9σ (C) or at 1σ (A, B, and D). The CO ligand and the side chains of Lys 96, Phe 97, and Asn 100 were omitted from the map calculations. All data to the limiting resolution were included in all four maps. Note the conformation of the phenyl side chain at position 97 and the presence or absence of ligand. This figure was produced with the programs BOBSCRIPT (*37*) and RASTER3D (*38*).

7 of the 11 water molecules being present and no water molecules distinct for the T-state present.

This transition structure suggests that attenuating the subunit rotation prevents formation of an interface in which the functionally important R-state interactions are stable. The heme group is central to this issue; while the heme group in each subunit approaches an R-state position the two heme groups do not achieve a full R-state separation (Table 2) and the A propionates cannot move to an extended R-state conformation without steric clashes at the interface. Thus, the ligand-linked subunit rotation is required for the heme groups to attain an R-state conformation.

Our results demonstrate that the crystal lattice of deoxy HbI restricts the structural transitions that occur upon ligand binding. It is intriguing that equilibrium oxygen binding experiments on deoxy HbI crystals showed full cooperativity (*11*). There are several possible explanations. It is conceivable that the full transitions are not required for full expression of cooperativity. This would appear unlikely given the

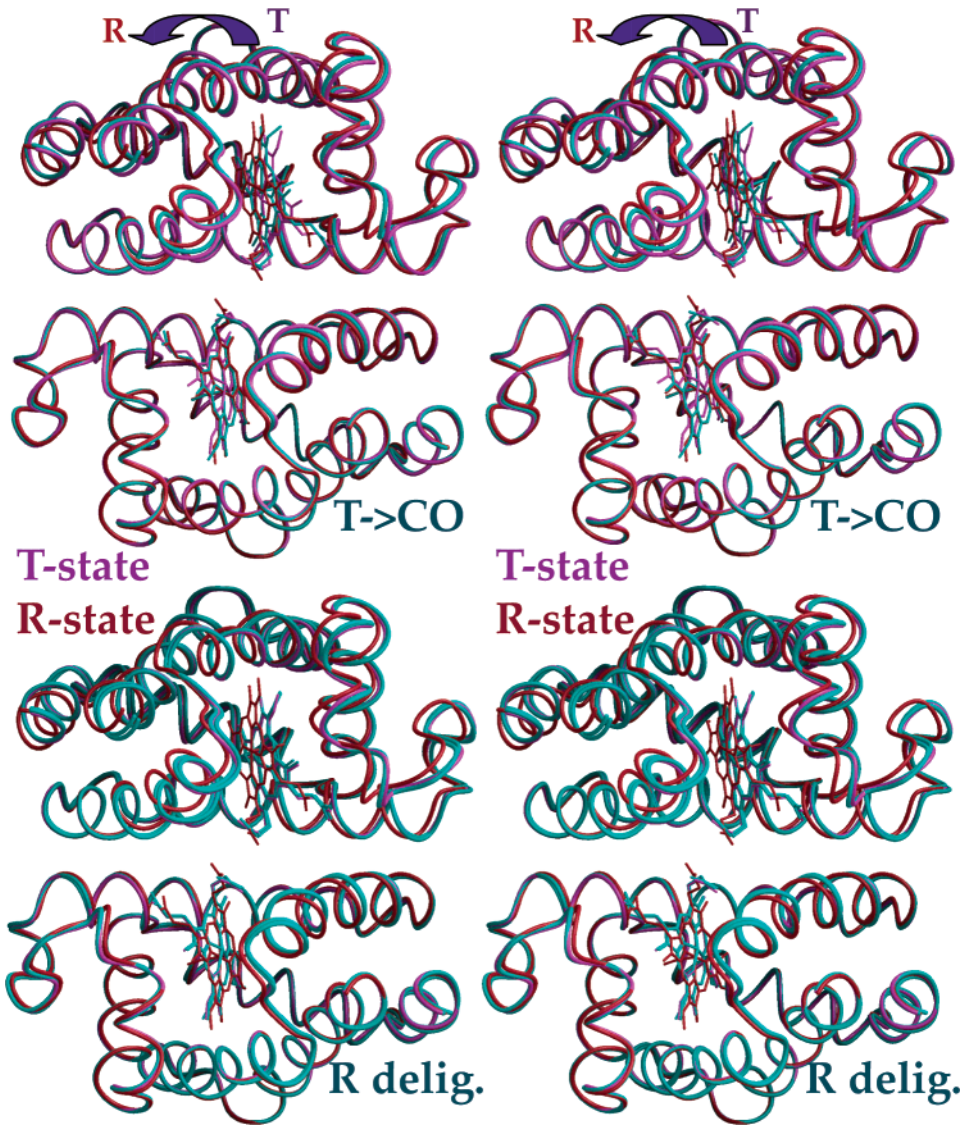

FIGURE 4: Stereoview of quaternary rearrangement of HbI and transition structures. The T-state (deoxy) structure is shown in magenta, R-state (CO) structure is shown in red and the transition structures are shown in cyan. An arrow at the top indicates the direction of the small ligand-linked subunit rotations. In both cases, the bottom subunits in each dimer have been superimposed. The T to CO transition structure is shown at the top (a). Note addition of CO to crystals grown in the deoxy state is coupled with an attenuated rotation of subunits. The R deligation transition structure is shown at the bottom (b). Removal of CO from subunits in the monoclinic lattice results in a quaternary structure that is almost identical with that of the T-state.

results on HbI−CO crystals (below) showing that in that crystal form the full quaternary change occurs despite lattice interactions that would, presumably, oppose such motions. It is a distinct possibility that the crystals used in the oxygen binding experiments did show some disruption of crystal lattice that was not evident by observing the crystals. In this regard, it is worth noting that our experiments in which crystals are exposed to CO while bathed in stabilizing solution always showed poor diffraction patterns, even though such changes in the internal order were not usually evident from observing the crystals in a microscope. Another possibility is that the much smaller crystals used for the oxygen binding experiments allow greater motion than those used for diffraction analysis.

R-State Deligation Transition. Crystals of HbI−CO were transformed into their unligated state by a two-step protocol in which the crystals were first oxidized to the cyanomet form before being reduced under anaerobic conditions to the unligated form. These crystals maintain sufficient order to allow collection of a diffraction data set to 2.5 Å, but undergo a transition to the primitive monoclinic space group $P2_1$. The relationship between the $C2$ and $P2_1$ lattices is shown in Figure 2. Although crystallographic C-centering is lost in the $P2_1$ cell, approximate C-centering is apparent from much stronger intensity of $h+k$ even reflections than $h+k$ odd reflections at low diffraction angles (Figure 6). With true crystallographic C-centering, the intensity will be zero for all $h+k$ odd reflections. Thus, the two dimers per asymmetric unit of the transition crystals are similar, but are no longer identically related by crystallographic $C2$ symmetry.

The atomic model for the structure of the transition crystal includes two dimers (designated AB and CD) and 147 ordered water molecules (Table 1). Electron density maps confirm the absence of a diatomic ligand at the heme groups (Figure 3B), and the geometry of all four heme groups (Table 2) is consistent with that of an unligated heme. The presence of a T-state structure extends to the overall tertiary structure (Table 2, Figure 5).

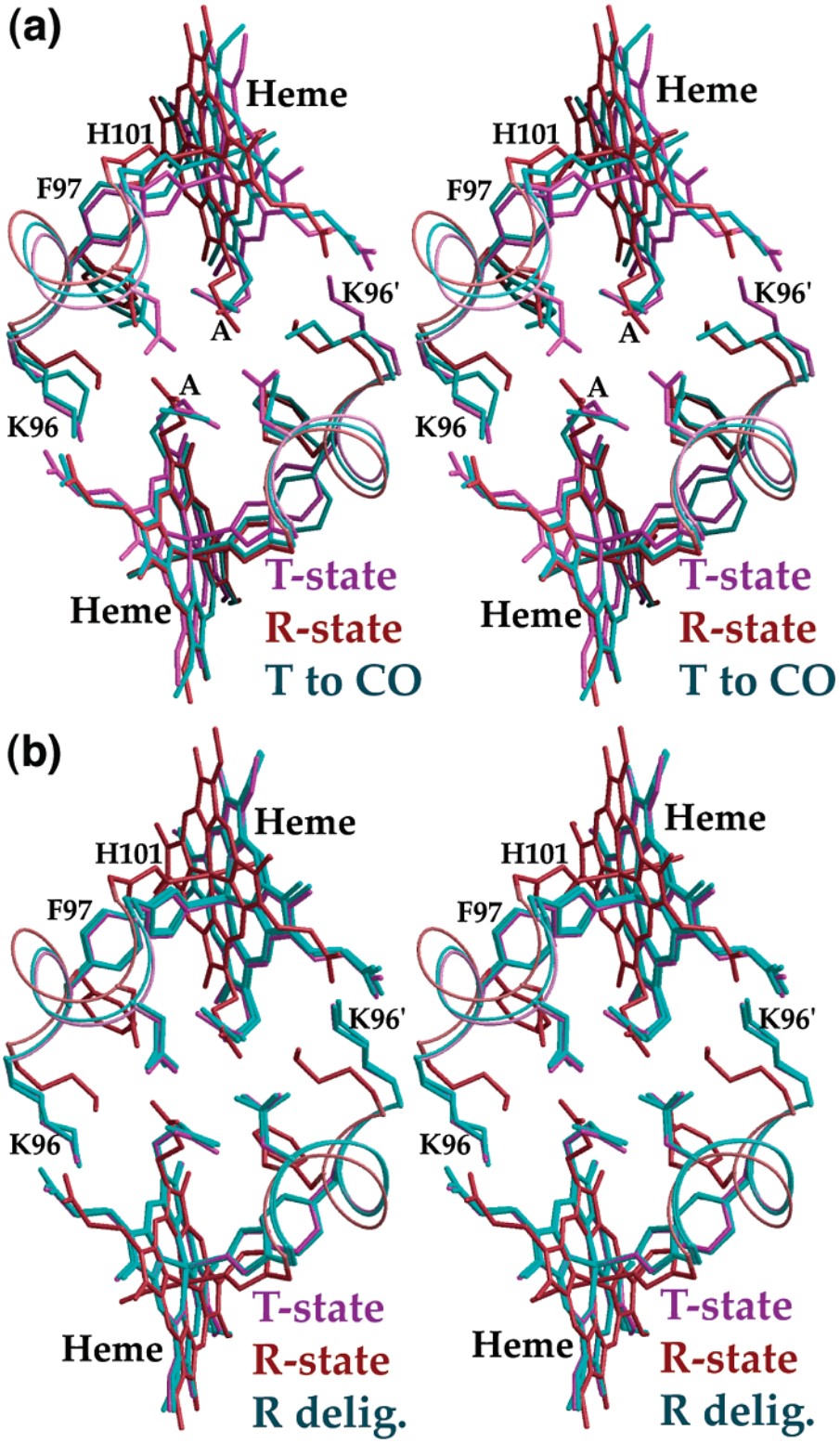

FIGURE 5: Stereodiagram showing structural comparisons of the T to CO (a) and R deligation (b) transitions. Each diagram includes a main-chain trace of residues 96 to 100, side chains for residues K96, F97, N100, and H101 and the heme group, with the T-state structure in magenta, R-state structure in red and transition structures in cyan. (Both AB and CD transition dimer structures are shown in the bottom panel.) Key residues are labeled, as are the A propionates (A) in the top figure. The lower subunits are aligned in each figure so that subunit tertiary changes are evident in the lower subunit, while the upper subunit has changes resulting from both tertiary and quaternary effects. The T to CO transition (a) achieves an intermediate structure, while the R deligation transition (b) is almost identical to the T-state structure.

Unlike the unligated to CO transition, the full allosteric transition occurs upon ligand release in these crystals. Key to the full transition is the ability of the lattice to tolerate quaternary subunit rearrangement with observed subunit rotations of 2.2° and 4.1° for the two dimers per asymmetric unit (Table 2, Figure 4).

Importantly, the structural conformations previously implicated in the low affinity of the T-state are observed.

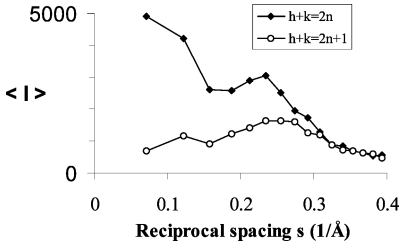

FIGURE 6: Plot of the mean intensity of reflections vs reciprocal spacing in the $P2_1$ transition structure. The much stronger intensity of the $h+k$ even reflections compared with the $h+k$ odd reflections indicates approximate C-centering remaining in the lattice. This effect is pronounced at low scattering angles but lost as higher angle reflections are considered. This plot is based on indexing reflections in the alternate lattice in which the cell axes are in the direction of the C2 lattice.

Functionally important T-state attributes confirmed by mutagenesis include the position of the heme groups (*23*), the conformation of Phe 97 (*24*), and the distribution of interface water molecules (9). The heme groups occupy nearly identical positions to those in the T-state (Figures 4b and 5b) with the relative heme distances within 0.1 Å of the T-state values (Table 2). Residues that interact with the heme group (Arg 53, Lys 96, Asn 100, and Arg 104) also assume T-state conformations in the transition crystal structure. Likewise, the side chain of Phe 97 side chain is in the T-state position in all four subunits, packed in the heme pocket in a manner that will reduce ligand binding affinity (Figure 5b). The core interface water cluster in the refined model is similar, but not identical, to that from crystals grown in the deoxy state, with 15 water molecules in the transition crystal structure, in comparison with 17 water molecules in the deoxy HbI structure and 11 in the HbI−CO structure. The small difference between the two unligated interface water structures may result more from the differences in resolution of the analyses (2.5 vs 1.6 Å) than any true difference in structure.

Reversibility of Ligand Transitions within Monoclinic HbI Crystals. Unligated transition crystals subsequently exposed to CO maintain sufficient order to allow collection of a diffraction data set to 2.8 Å. Analysis of diffraction patterns collected following exposure to CO indicated that these crystals undergo a slow transition (~ 10 h) from the transition $P2_1$ lattice back to the original C2 cell of HbI−CO. An atomic model was refined using tight noncrystallographic restraints between the two subunits of the dimer, due to the limited resolution of the data (Table 1).

Examination of the electron density from both $F_o - F_c$ and $2F_o - F_c$ σ^A weighted maps showed the presence of large positive peaks above the heme groups, indicating that the CO ligand is bound (Figure 3C). Further examination of the electron density maps showed that the double transition structure adopts a high ligand-affinity like structure with the aromatic side chain of Phe 97, the heme groups and subunit interface residues positioned in their R-state locations (Table 2). The quaternary assembly is R-like, but differs by 1.0° from the assembly of the starting CO-ligated structure. Thus, the double transition structure demonstrates that the ligand transitions are reversible within the monoclinic lattice.

Crystal Lattice Transitions. The crystal lattices of ligated and unligated HbI have distinctly different responses to alterations in the ligand state. The greater ability of the monoclinic HbI−CO crystals to accommodate quaternary structural transitions may be due, in part, to the lower crystallographic symmetry of the monoclinic lattice relative to that in the orthorhombic crystal lattice. The limited subunit rotation upon binding CO in the orthorhombic lattice of unligated HbI results in very little alteration in crystal packing, with individual lattice contact distances changing by an average of 0.24 Å. Superimposing the HbI−CO dimer onto deoxy HbI shows that a number of unfavorable contacts would result in the $C222_1$ lattice if HbI undergoes a full T- to R-state transition. Specifically, a total of five steric clashes (crystal packing contacts with atomic distances between 1.9 and 2.5 Å) and 13 bad contacts (non-hydrogen bonded atoms with distances between 2.5 and 3.0 Å) would occur. Furthermore, many of these unfavorable or forbidden contacts involve main chain atoms, and would require major rearrangements to accommodate the allosteric transition.

In contrast, the monoclinic *C*2 lattice of HbI−CO can accommodate the full quaternary R → T transition. In doing so, the lattice converts from *C*2 to $P2_1$ symmetry as the quaternary change drives the loss of the crystallographic 2-fold axes along *b*, replacing them with quasi 2-fold axes that are tilted 1° from the crystallographic *b* axis (Figure 1). Most of the lattice contacts involve side chains that are sufficiently flexible to accommodate the small quaternary rotation. However, there are 18 out of 52 unique crystal packing interactions that involve less flexible main chain atoms. In 14 of these 18 the contacting distance either remains the same, or increases slightly. The remaining four contacts have distances that decrease by less than 0.1 Å, providing no steric barrier to inhibit the quaternary change. Surprisingly, the double transition does not restore the original packing contacts, but rather differ more from those observed in the starting HbI−CO structure than do those in the unligated transition structure.

Crystal Lattice Impact on Allosteric Protein Transition. The degree to which a crystal lattice alters protein conformation is a legitimate concern especially when considering allosteric proteins for which alternate structural conformations must be accessible under physiological conditions. Therefore, it can be quite instructive to follow structural changes that are permitted within the crystal lattice. In the case of human hemoglobin, structures have been obtained upon binding oxygen to unligated crystals grown from poly(ethylene glycol). These studies have illuminated stereochemistry of low affinity binding to human hemoglobin (*25*, *26*), as the crystallized hemoglobin maintains the T-state in the presence of oxygen (*27*−*29*). Similarly, the structure of crystals of lamprey hemoglobin grown in the unligated state but subsequently exposed to CO has revealed the stereochemistry of binding to the low affinity assembled form of this molecule (*30*). However, concerted structural transitions can occur upon ligand binding in protein crystals, such as evidenced by the binding interactions among dichloroethane, protons, and SO_4^{-2} ions in cubic insulin crystals (*31*). Additionally, following the diffraction patterns of asparate transcabamoylase grown in the absence of substrate but subsequently soaked with aspartate indicated a slow transformation of this crystal lattice (*32*). An interesting example of the impact of a crystal lattice on structure is lactate dehydrogenase from the anaerobic bacterium, *Bifidobacterium longum* (*33*). Although crystallization of this allosteric

enzyme was carried out under solution conditions that strongly favor the R-state form, the crystals formed were found to contain an equimolar ratio of both R- and T-state molecules. Thus, fortuitously, this analysis provided both allosteric states in a single crystal, minimizing the differences in conditions for comparison of allosteric changes. However, the analysis also clearly demonstrates the ability of a crystal lattice to dramatically alter the equilibrium between alternate conformational states of an allosteric protein.

A direct impact of the crystal lattice on allosteric transitions is evident in the structure of unligated *Scapharca* HbI crystals exposed to CO. Ligand binding produces a structure that is intermediate between that of the T- and R-state, as the orthorhombic lattice restrains the full quaternary structural transition. The lattice restricts the rotation of subunits to about 20% of the T to R transition, but still permits heme movements of about 75% of the T to R transition. Importantly, this heme movement is not sufficient to allow its propionates to acquire an R-state conformation in the dimeric interface.

The monoclinic lattice of ligated HbI crystals is, however, able to maintain sufficient internal order as complete allosteric transitions occur. These transitions include all aspects that have been previously identified by mutagenesis as important for the allosteric mechanism of HbI. In addition, the small quaternary rearrangement of subunits was unexpectedly found to occur even in the presence of lattice interactions that would likely oppose such motion. Previously, it was unclear whether the quaternary rearrangement was linked to ligand binding, or resulted from differences in lattice interactions between the unligated and ligated crystal forms. The transitions observed in the monoclinic crystal form indicate that this quaternary rearrangement, although small, is an integral aspect of the allosteric transitions in *Scapharca* HbI. Moreover, comparison with the unligated to CO transition suggests that the degree of reorientation between subunits is coupled with the extent of the ligand-linked heme movement. Such a conclusion is consistent with previous structural analysis of mutants of HbI, which show mutations that alter the interface water structure (*34*) or Phe 97 (*24*) undergo the full wild-type quaternary transitions, but that these transitions are restricted when the heme movement is limited (*23*).

The ability to follow complete cooperative structural transitions within the crystal lattice strongly supports the earlier conclusions concerning the allosteric mechanism of *Scapharca* HbI. As well, they show that a protein crystal lattice can be sufficiently plastic to permit limited cooperative transitions. Finally, this work suggests that the monoclinic lattice may be a particularly amenable system for following allosteric transitions as they occur. Such nanosecond time-resolved crystallographic experiments on HbI−CO crystals are currently underway.

ACKNOWLEDGMENT

We thank Dr. Balaji Bhyravbhatla for helpful discussions.

REFERENCES

1. Holt, J. M., and Ackers, G. K. (1995) *FASEB J. 9*, 210−218.
2. Shaanan, B. (1983) *J. Mol. Biol. 171*, 31−59.
3. Smith, F. R., and Simmons, K. C. (1994) *Proteins 18*, 295−300.
4. Silva, M. M., Rogers, P. H., and Arnone, A. (1992) *J. Biol. Chem. 267*, 17248−17256.
5. Haurowitz, F. (1938) *Hoppe Seylers Z. Physiol. Chem. 254*, 266−274.
6. Liddington, R., Derewenda, Z., Dodson, G., and Harris, D. (1988) *Nature 331*, 725−728.
7. Chiancone, E., Vecchini, P., Verzili, D., Ascoli, F., and Antonini, E. (1981) *J. Mol. Biol. 152*, 577−592.
8. Antonini, E., Ascoli, F., Brunori, M., Chiancone, E., Verzili, D., Morris, R. J., and Gibson, Q. H. (1984) *J. Biol. Chem. 259*, 6730−6738.
9. Royer, W. E., Jr., Pardanani, A., Gibson, Q. H., Peterson, E. S., and Friedman, J. M. (1996) *Proc. Natl. Acad. Sci. U.S.A. 93*, 14526−14531.
10. Monod, J., Wyman, J., and Changeux, J.-P. (1965) *J. Mol. Biol. 12*, 88−118.
11. Mozzarelli, A., Bettati, S., Rivetti, C., Rossi, G. L., Colotti, G., and Chiancone, E. (1996) *J. Biol. Chem. 271*, 3627−3632.
12. Summerford, C. M., Pardanani, A., Betts, A. H., Poteete, A. R., Colotti, G., and Royer, W. E., Jr. (1995) *Protein Eng. 8*, 593−599.
13. Royer, W. E., Jr. (1994) *J. Mol. Biol. 235*, 657−681.
14. Otwinowski, Z., and Minor, W. (1997) *Methods Enzymol. 276*, 307−326.
15. Kissinger, C. R., Gehlhaar, D. K., and Fogel, D. B. (1999) *Acta. Crystallogr. D Biol. Crystallogr. 55 (Pt 2)*, 484−491.
16. Brunger, A. T., Adams, P. D., Clore, G. M., DeLano, W. L., Gros, P., Grosse-Kunstleve, R. W., Jiang, J. S., Kuszewski, J., Nilges, M., Pannu, N. S., Read, R. J., Rice, L. M., Simonson, T., and Warren, G. L. (1998) *Acta Crystallogr. D Biol. Crystallogr. 54 (Pt 5)*, 905−921.
17. Jones, T. A., Zou, J. Y., Cowan, S. W., and Kjerdgaard, M. (1991) *Acta Crystallogr. A47*, 110−119.
18. Kleywegt, G. J., and Jones, T. A. (1996) *Structure 4*, 1395−1400.
19. Kleywegt, G. J. (1996) *Acta Crystallogr. D52*, 842−857.
20. Collaborative Computational Project No. 4 (1994) *Acta Crystallogr. D50*, 760−763.
21. Berman, H. M., Westbrook, J., Feng, Z., Gilliland, G., Bhat, T. N., Weissig, H., Shindyalov, I. N., and Bourne, P. E. (2000) *Nucleic Acids Res. 28*, 235−242.
22. Condon, P. J., and Royer, W. E., Jr. (1994) *J. Biol. Chem. 269*, 25259−25267.
23. Knapp, J. E., Gibson, Q. H., Cushing, L., and Royer, W. E., Jr. (2001) *Biochemistry 40*, 14795−14805.
24. Pardanani, A., Gibson, Q. H., Colotti, G., and Royer, W. E., Jr. (1997) *J. Biol. Chem. 272*, 13171−13179.
25. Mozzarelli, A., Rivetti, C., Rossi, G. L., Henry, E. R., and Eaton, W. A. (1991) *Nature 351*, 416−419.
26. Rivetti, C., Mozzarelli, A., Rossi, G. L., Henry, E. R., and Eaton, W. A. (1993) *Biochemistry 32*, 2888−2906.
27. Luisi, B., Liddington, B., Fermi, G., and Shibayama, N. (1990) *J. Mol. Biol. 214*, 7−14.
28. Liddington, R., Derewenda, Z., Dodson, E., Hubbard, R., and Dodson, G. (1992) *J. Mol. Biol. 228*, 551−579.
29. Paoli, M., Liddington, R., Tame, J., Wilkinson, A., and Dodson, G. (1996) *J. Mol. Biol. 256*, 775−792.
30. Heaslet, H. A., and Royer, W. E., Jr. (2001) *J. Biol. Chem. 276*, 26230−26236.
31. Gursky, O., Fontano, E., Bhyravbhatla, B., and Caspar, D. L. (1994) *Proc. Natl. Acad. Sci. U.S.A. 91*, 12388−12392.
32. Gouaux, J. E., and Lipscomb, W. N. (1989) *Proc. Natl. Acad. Sci. U.S.A. 86*, 845−848.
33. Iwata, S., Kamata, K., Yoshida, S., Minowa, T., and Ohta, T. (1994) *Nat. Struct. Biol. 1*, 176−185.
34. Pardanani, A., Gambacurta, A., Ascoli, F., and Royer, W. E., Jr. (1998) *J. Mol. Biol. 284*, 729−739.
35. Kraulis, P. J. (1991) *J. Appl. Crystallogr. 24*, 946−950.
36. Ferrin, T. E., Huang, C. C., Jarvis, L. E., and Langridge, R. (1988) *J. Mol. Graphics 15*, 13−27.
37. Esnouf, R. M. (1997) *J. Mol. Graphics 15*, 132−134.
38. Merritt, E. A., and Bacon, D. J. (1997) *Methods Enzymol. 277*, 505−524.

BI027136P